Discrimination of benign-*versus*-malignant skin lesions by thermographic images using support vector machine classifier

Mirian Denise Stringasci,[1,a)] Ana Gabriela Salvio,[2] David Sbrissa Neto,[1,3] José Dirceu Vollet-Filho,[1] Vanderlei Salvador Bagnato,[1] and Cristina Kurachi[1]
[1]*São Carlos Institute of Physics, University of São Paulo (USP), PO Box 369, 13560-970 São Carlos, São Paulo, Brazil*
[2]*Skin Department, Amaral Carvalho Foundation, Jau, Brazil*
[3]*Science and Technology Department, Federal University of Amapa (UNIFAP), 68903-419 Macapá, Amapá, Brazil*

(Received 17 April 2018; accepted 11 July 2018; published online 30 July 2018)

Skin cancer is the cancer type with the highest incidence in the world. Its diagnosis requires a specialist physician, with expertise in skin diagnostics. Thermography is a noninvasive technique based on the detection of infrared emission that is completely safe to humans. In this study, thermal images of clinically similar lesions were registered and analyzed aiming to provide a noninvasive diagnostic information for discrimination of: basal cell carcinoma *versus* intradermal nevus, squamous cell carcinoma *versus* actinic keratosis, and melanoma *versus* pigmented seborrheic keratosis. Thermal images were analyzed using a MATLAB® routine to evaluate statistical, histogram, and filtering metrics of each image, and a support vector machine classifier was used to discriminate the lesions based on those metrics values. Actinic keratoses and squamous cell carcinoma showed distinct average temperatures, whereas the other pairs of lesions presented similar temperatures. Nevertheless, the benign lesions showed higher definition of borders detection than malignant lesions, as a general rule. The results showed that support vector machine classifier has great ability for discrimination of clinically similar lesions based on their thermal images, suggesting that the thermography can be used as an auxiliary tool for the diagnosis of skin malignant lesions. *Published by AIP Publishing*. https://doi.org/10.1063/1.5036640

I. INTRODUCTION

Skin cancer is the cancer type with the highest incidence in the world.[1] In Brazil, approximately 176 000 new cases of non-melanoma skin cancer are expected in 2016, corresponding to 25% of all malignant tumors registered in the country; 5670 new cases of melanoma are also expected for this year, and 1547 patients will die from the disease.[2]

The non-melanoma cancer subtypes are the basal cell carcinoma (BCC) and squamous cell carcinoma (SCC).[3] BCC is the most common type of non-melanoma skin cancer, representing approximately 80% of the cases. Although BCC grows slowly and rarely metastasizes, it presents a morbidity problem, since it often appears as multiple lesions and a relevant economic issue for the health system.[4–6] SCC, the second most common skin cancer, has an invasive character and can metastasize. SCC primary lesion can change continuous and progressively from non-invasive lesions, named actinic keratoses (AKs), so diagnosing the lesion during this process is a challenge because the features of both lesions may be simultaneously present in the region.[4–6]

Melanoma is the most aggressive skin cancer, and although its incidence is low, this disease shows a high mortality rate.[7] Pigmented Seborrheic Keratosis (PSK), on the other hand, is a benign and common lesion that sometimes even for the most experienced dermatologist can clinically mimic a malignant melanoma.[8] As the same way, some nevi may be indistinguishable from a normochromic intradermal nevus (NI). The clinical diagnostic is performed with visual macroscopic inspection and when a lesion is detected, an enhanced visualization by dermoscopy is used by dermatologists. Dermoscopy is a non-invasive optical instrument, based in microscopy, which uses incident light and oil immersion to allow the observer looking into the superficial skin layers, making subsurface structures accessible to visual examination *in vivo*.[9,10] The gold standard for skin diagnostics is histopathology.[11] In developing countries, most of the population has little to none access to medical specialists, and by consequence, patients often end up not receiving or facing a long waiting period for the correct diagnosis. In Brazil, 52.9% of the cities do not offer pathology facilities for patient analysis of primary care.[12] This is particularly alarming, where the cancer diagnosis at early stages, increases the chance of complete healing and less morbidity. This is particularly important especially in cases of surgery, where early diagnosis usually implies in small tumor tissue volume, facilitating complete removal with tumor free margins.[2]

Diagnosis techniques by fluorescence and reflectance microscopy are some of the examples of optical techniques to identify several diseases. Fluorescence reflects chemical and physical changes occurring in tissue. Since different tissues or different conditions of the same tissue have distinct endogenous fluorescence emission, it can be used as a detection method to improve the accuracy in diagnosis.[13]

[a)]Author to whom correspondence should be addressed: mirianstringasci@gmail.com

Fluorescence, by both spectroscopy and widefield imaging methods, has the ability to reveal cancer lesions as well as cancerization areas.[14] Confocal reflectance microscopy provides images from very well-defined focus in different focal planes, providing high resolution images. Although there are commercial devices that provide viable tissue images with high-resolution and contrast without performing a biopsy or processing a tissue sample, as in standard histology, high costs are involved.[15,16] These techniques are harmless and non-invasive and do not cause pain or discomfort to the patient. None of those techniques will replace histopathology as a gold standard but may provide physicians with tools for discrimination between malignant and benign lesions, minimizing costs, and time for diagnosis.

Factors such as metabolic rate and blood perfusion, in special when considering abnormal cells, affect the body surface temperature. Malignant tumor cells may thus present local temperature variations if compared with other lesions, due to increased metabolic rate and vascularization.[17–19] Therefore, a possible approach for the assessment of cancer lesions is the use of thermography techniques. In thermography, the temperature at the body surface is measured and presented as an image in which a temperature value is measured and attributed to each pixel. This technique records body temperature distribution by using the infrared radiation emitted from the surface of this body, in wavelengths that range between 7 and 14 μm.[20] The interest in using this technique as a diagnostic approach is increasing because this is a noninvasive technique and completely safe to humans as it involves solely detecting the infrared radiation naturally emitted by the tissues. This technique has been broadly studied and developed to diagnose breast cancer.[20–22] Another benefit in presenting thermography as an optical technique is that there are devices ranging within all sort of price variations, from simple cellular adapters to expensive refrigerated cameras.[23] There are studies in dermatology reported in the literature that suggest that high temperature is observed in aggressive tumors such as melanoma; however, to the best of our knowledge, no study shows temperature changes in a quantitatively manner, allowing for discrimination of these tumors when considering clinically similar lesions.[24,25] Nonetheless, the differences between lesions' temperature are sometimes too subtle to be promptly identified, which means that an accurate and trustworthy use of this approach demands adequate methods for the discrimination of similar thermal images.

The aim of this study is to evaluate the ability of thermography to discriminate clinically similar lesions. The thermal images of—BCC *versus* NI, SCC *versus* AK, and melanoma *versus* PSK—lesions were recorded and compared two-by-two by exploring a processing mathematical method called support vector machine (SVM). SVM is a machine learning technique, which originates from statistical theory and has been widely used in pattern recognition applications because of its computational efficiency and good performance. The main advantage of SVM is an ability to model highly nonlinear systems and find an efficient separation between them from surface properties.[26–28]

II. MATERIAL AND METHODS

The infrared images were obtained using a thermal imager with infrared lens (Fluke® FLK-Ti400 model), with thermal sensitivity $\leq 0.05\,^{\circ}$C, precision of $\pm 2\,^{\circ}$C, image capture frequency of 60 Hz, and 320 $\times$ 240 pixels resolution.[29] The equipment accuracy is $\pm 2\,^{\circ}$C. However, the metrics analyzed variances within the image itself, i.e., among pixels, for which the sensitivity is of at least 0.05 °C. Thus, the low accuracy for temperature values does not interfere with the analyses, which will depend on the high sensitivity instead.

The imager detects simultaneously the visible light and infrared ranges of the spectrum and shows the image of choice on its own display, avoiding the need of coupling to a computer. The device also presents auto focus adjustment feature, and the screen displays a color scale for the temperatures displayed, and the option to use markers that indicate the temperature at specific locations. The images can be downloaded to the computer and edited through the dedicated software Fluke SmartView 3.5, which allows saving files as thermography image, the visible light image (that is also registered simultaneously to thermal image), or as a matrix of the temperature values for each pixel.

Data collection was performed at Skin Department of Amaral Carvalho Hospital Foundation in Jahu – SP under supervision of Dr. Ana Gabriela Salvio. Patients were hosted at a room with temperature set at 22 °C for 10 min before thermography imaging. Lesions with fluids were cleaned with dry gauze only. The patient was made comfortable and the thermal imager was positioned at a distance of 15 cm from the lesion (which is the minimum distance for the focus of the device). A sticker with a millimeter scale was attached close to the lesion as a reference for the lesion size in the images, and the thermal imager collected both thermal and white light images.

The interrogated lesions were: 100 BCC, 100 NI, 35 SCC, 35 AK, 20 PSK, and 20 melanomas. The difference in the numbers for each type of lesion is due to their distinct incidence rates. The diagnosis was confirmed by the dermatologist (A.G.S.) and by histopathology, and the enrolled patients agreed and signed an informed consent form. The thermal images analysis was performed using a routine elaborated in MATLAB® (R2009a, MathWorks, United States).

A. Image processing and analysis

In order to analyze the temperature and its behavior as a factor of discrimination between two distinct pathologies, image processing and analysis techniques were applied to the obtained dataset. The algorithm was performed in MATLAB® software and previous analysis was done in Weka® 3.8 (1999–2016, The University of Waikato, New Zealand).

First, the images were manually cropped. Each image was cropped as to preserve for analysis a region including only the lesion itself and a margin of approximately 2 mm from the edge. There were redundancies (unnecessarily selected parts of the image, e.g., when a healthy tissue area is proportionally much larger than the lesion area) and

TABLE I. Metrics used in routine elaborated in MATLAB®.

Statistical attributes		
Entropy	$H = \sum_i p_i . \log(p_i)$[a]	Disorder degree of the image
Maximum minus minimum	$T_{max} - T_{min}$	Difference between maximum and minimum temperature
Mean[b]	$\overline{T} = \frac{1}{N}\sum_{i=1}^{N} T_i$	Average of N temperature pixels
Std[b]	$\sigma_T = \sqrt{\frac{\sum_i^N (T_i - \overline{T})^2}{N-1}}$	Standard deviation of temperatures
Cv	$cv = \frac{\sigma_T}{\overline{T}}$	Coefficient of variation
Skewness	$S = \frac{E(T_i - \overline{T})^3}{\sigma_T^3}$[c]	Asymmetry of temperature distribution
Kurt[b]	$k = \frac{E(T_i - \overline{T})^4}{\sigma_T^4}$	Asymmetry of temperature distribution
Contrast[b]	$\sum_i \sum_j (i-j)^2 . glcm(i,j)$[d]	
Correlation	$\frac{\sum_i \sum_j (i-\overline{i})(j-\overline{j}) glcm(i,j)}{\sigma_i \sigma_j}$	
Energy[b]	$\sum_i \sum_j glcm(i,j)^2$	
Homogeneity	$\frac{\sum_i \sum_j glcm(i,j)}{1+\lvert i-j \rvert}$	
Histogram analysis		
zcoef1[b]	$h(T) = zcoef1.T^2 + zcoef2.T + zcoef3$	Histogram polynomial regression zero-excluded – 2nd order
zcoef2		
zcoef3[b]		
coef1[b]	$h(T) = coef1.T^2 + coef2.T + coef3$	Histogram polynomial regression – 2nd order
coef2		
coef3		
Skin-lesions interface		
DenFor1	…	Average temperature inside divided by average temperature outside by Otsu segmentation
DenFor2	…	Average temperature edge divided by average temperature outside "Prewitt" filter
DenFor3	…	Average temperature edge divided by average temperature outside "Roberts" filter
DenFor4[b]	…	Average temperature inside divided by average temperature outside by Weight pixel segmentation
Edge1	…	Temperature average of the edge "Prewitt" filter
Edge2	…	Temperature average of the edge "Roberts" filter

[a] $p(i)$ is normalized histogram of the image.[34]
[b] Attributes selected by the classifier method.
[c] $E(t)$ represents the expected value of a variable t.[34]
[d] i and j represent row and column dimensions of the image, and $glcm(i, j)$ represents gray-level cooccurrence matrix.[34]

obstructions (artifacts from image collection, e.g., pieces of cloth, hair, or anatomical elements—eye, ear, etc.) to the image collection such as body hair strand and skin surface unevenness. Those elements produce image artifacts interfering on the analysis of the lesion and its surroundings. Thus, an attribute selection was performed based on the characteristics of the lesions' images. Several attributes of lesions were explored to contribute to the classes' discrimination. Assuming T_i as the temperature value of each point in an image, the following group of characteristics was evaluated: Statistical Attributes, Histogram Analysis, and Skin-Lesion Interface (Table I).

Statistical Attributes represent the statistical analysis of the temperature values for each image, using as attributes eleven usual statistical parameters, namely: entropy, maximum-minimum subtraction ("maximum minus minimum"), mean, standard deviation, variation coefficient, skewness, kurtosis, contrast, correlation, energy, and homogeneity.[30–32] In addition, texture contrast, correlation energy, and homogeneity attributes were calculated, where a co-occurrence matrix for neighboring pixels was extracted for $\theta = 0°$ and $d = 1$.[33,34] Histogram analysis is based on the values of the temperature histogram of each image. Each image histogram was fitted by a second-order polynomial equation, since the histogram best fits a parabola. The equation coefficients obtained were used as attributes. Skin-lesions interface represents filters that were used to select only the lesion region and to differentiate this region from the healthy skin. The filters chosen for this analysis are Otsu and Weight segmentations and Prewitt and Roberts filters.[30–32]

For this, comparison attributes were defined using the average temperature within and outside the lesion borders, with borders identified by the different filters applied by each attribute ("Skin-lesions interface"). All the attributes are shown and described in Table I. The attributes indicated with "**b**" in Table I are those that actually contributed to the discrimination of the pairs, which were selected by the classifier.

B. Classification

Support Vector Machine (SVM) is a useful technique for many multidimensional classification problems. Like

other techniques, the main goal of SVM is to build a model which predicts the target values for the test set based on it features. The goal of two-class classification problem using linear model is design a hyperplane

$$y(x) = w^T \varphi(x) + b,$$

which classifies all the training data correctly. Let a training set be $(\mathbf{x}_i, t_i)$, $i = 1, \ldots, l$, where $\mathbf{x}_i$ is a feature vector and t_i is the label class from the ith sample. If $t_i = +1$ is the benign class, the vector x_i satisfies $y(x_i) > 0$, if $t_i = -1$, $y(x_i) < 0$ and $\mathbf{x}_i$ belongs to a malignant class. SVM algorithm approaches the problem by applying the concept of margin, defined by the smallest perpendicular distance between the decision boundary and the closest data points. Assuming that the distance of a point to a hyperplane is given by $\frac{|y(x)|}{\|w\|}$, the main idea through SVM algorithm solution is search the parameters w and b of the hyperplane that provides the maximum possible margin. The optimization problem can be summarized by

$$\min_{w,b,\xi} \frac{1}{2} \boldsymbol{w}^T \boldsymbol{w} + C \sum_{i=1}^{l} \xi_i,$$

subject to

$$t_i \left(w^T \varphi(x) + b \right) \geq 1 - \xi_i,$$

where C is an error parameter and ξ_i represents penalties for the *i*-th point that transgressed the margin.[26–28]

The solution of this problem requires a kernel function given by $K(\mathbf{x}_i, \mathbf{x}_j) = \varphi^T(\mathbf{x}_i)\, \varphi(\mathbf{x}_j)$. In the present study, we chose a linear kernel $K(\mathbf{x}_i, \mathbf{x}_j) = \mathbf{x}_i^T\, \mathbf{x}_j$.[35] The SVM algorithm was performed with software Weka® 3.8 (1999–2016, The University of Waikato, New Zealand).

C. Validation

Sensitivity is the term that defines how well the method is effective in correctly identifying the lesions evaluated, which means those that actually present the characteristic of interest, in this case the neoplastic lesions ("true positives"). The specificity of a method instead defines how effective it is to correctly identify individuals who do not present the condition of interest, which means non-neoplastic lesion in this case ("true negatives"). Sensitivity and specificity show better discrimination power when they reach closer to 1, that is, 100%.[36]

In a confusion matrix, all the cases of a model in categories are classified, determining if the predicted value corresponded to the real value. The rows in the matrix represent the predicted values and the columns represent the real values. False positive, true positive, false negative, and true negative terms are used to classify the values of the matrix.[37,38] Thus, for this study, the validation of choice was the *k*-fold method using a value of $k = 10$.

III. RESULTS AND DISCUSSION

A. BCC versus NI lesions

Figure 1 presents examples of thermal images of nodular BCC and NI. BCC lesions in thermal images presented lower temperature than their surrounding healthy tissue [Fig. 1(a)]. Such observation is in agreement with a study published by Buzug *et al.*[19] This study showed a single thermal image of a BCC lesion, selected from the original image by active contour and comparing temperatures within and outside the lesion spot. In their study, the temperature within the lesion border is smaller than for the surrounding tissue. They also show that when this lesion is cooled (by heat transfer to the skin) to a temperature of 27 °C, the thermal recovery is also slower than for the surrounding healthy tissue, which they associate to the fact that these carcinomas are poorly vascularized lesions. Similarly, NI lesions showed lower temperature than the surrounding tissue [Fig. 1(c)], but temperature difference from normal tissue was more prominent, so that the contour of lesion borders is better defined at the thermal images since an increased contrast is observed.

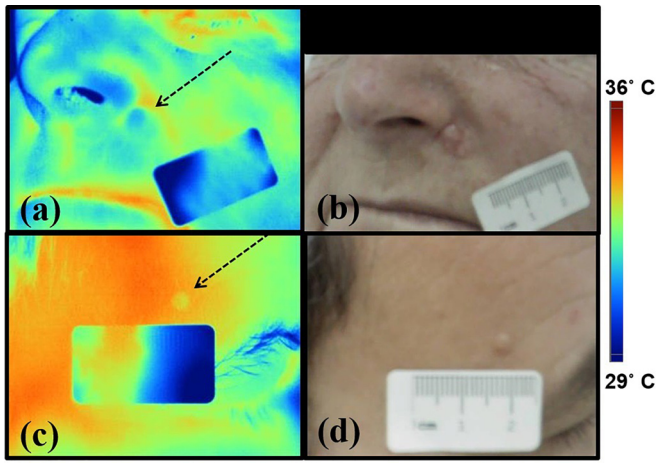

FIG. 1. (a) and (b) The thermal and white light images of a BCC lesion and (c) and (d) the thermal and white light images of an NI lesion, respectively.

B. SCC versus AK lesions

AK lesions can evolve into SCC lesions. The difficulty in discriminating these lesions relies on the fact that malignant progression occurs continuously, so that the features of both pathologies may be simultaneously present in the site, increasing the complexity of dermoscopy diagnostics.[39]

However, from the lesions compared in this study, this pair presented the greatest visual contrast at the raw thermal images. SCC region has generally higher temperature within the lesion site and at its surroundings [Fig. 2(a)]. This is probably due to the characteristic fast growing and to the increased aggressiveness of those lesions, which also increases angiogenic factors,[40] whereas thermal images of AK showed almost no difference in temperature when compared to the surrounding region, as one can see in Fig. 2(c).

To the best of our knowledge, no studies aiming to discriminate SCC and AK lesions were found in literature using temperature detection to date.[4–6] Since AK lesions may evolve undetected to SCC lesions, this first approach towards discriminating the lesion staging is important for clinical assessment, as its outcome could provide a non-invasive method to detect SCC almost in real-time If proven with high sensitivity and specificity rates, the thermography

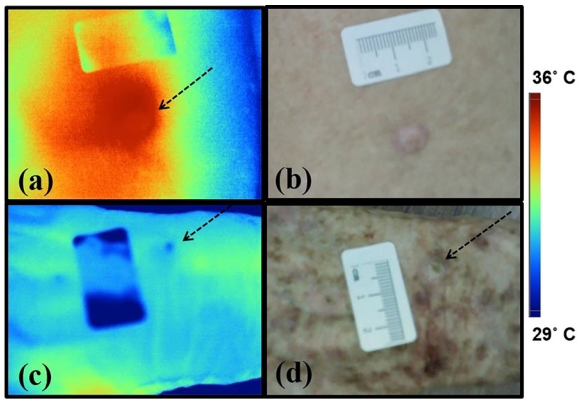

FIG. 2. (a) and (b) The thermal and white light images of a SCC lesion; and (c) and (d) the thermal and white light images of an AK lesion, respectively.

may constitute an important auxiliary diagnostic tool for skin cancer screening due to a fast response and large area interrogation evaluation.

C. Melanoma versus PSK lesions

Thermal images of primary cutaneous melanoma showed lower temperature within the area of the lesion when compared to its surrounding tissue, with ill-defined borders [Fig. 3(a)], while PSK lesions, which are benign lesions, presented higher contrast between lesion/normal tissue, i.e., an even lower temperature than the surrounding region, and more well-defined borders for most of the lesions, as seen in Fig. 3(c).

Melanoma has characteristic high aggressiveness and potential for metastasis. The metabolical conditions that favor these features are also usually responsible for an increase in the temperature. However, we can observe from our data that the temperature of the primary cutaneous melanoma lesion is lower than the one for the area surrounding it, and the lesion borders are usually quite diffuse. However, melanoma subcutaneous metastasis were also recorded by thermal images and showed higher temperatures with respect to the adjacent tissue [Fig. 4(a)]. This observation is in agreement with the study of Shada *et al.*, as they suggest that

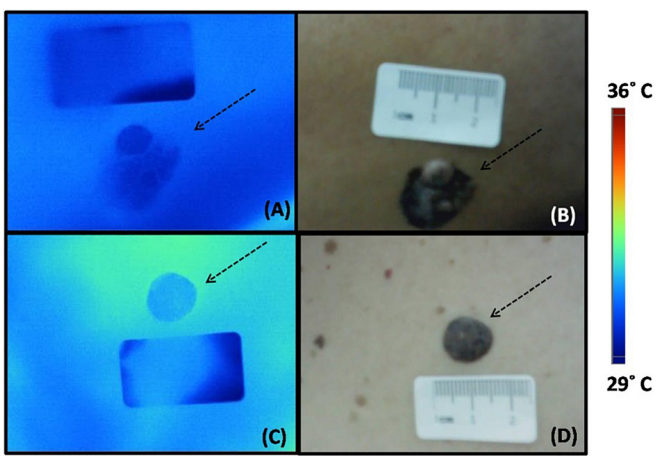

FIG. 3. (a) and (b) The thermal and white light images of a melanoma lesion; and (c) and (d) the thermal and white light images of a PSK lesion, respectively.

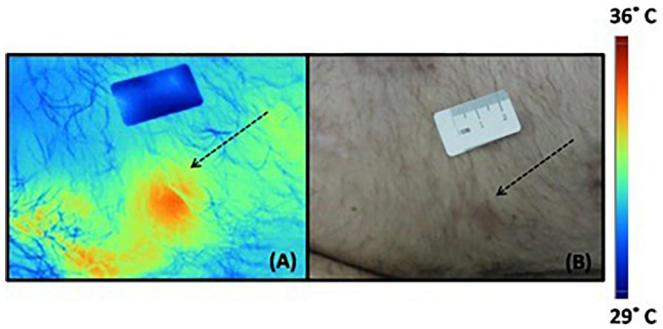

FIG. 4. (a) Thermal image and (b) white light of a subcutaneous melanoma lesion.

small and primary melanoma lesions have limited neovascularization and/or rapid dissipation of heat.[25]

D. Support vector machine as classifier

After visual analysis, the thermal images were evaluated by using a routine elaborated in MATLAB® to produce matrices that store the attributes information for each image. These matrices were submitted to analysis by the SVM classifier (from the Weka® software). This classifier correlated the attributes provided in the matrices using several methods, searching for the best method to differentiate images, separating them in one of the two types of lesions.

The SVM classifier determines the best separation method for each pair of lesions. The flowcharts obtained for each pair by using the attributes values are presented in Fig. 5. Although we have stored 23 attributes to the classifier, we could observe that only some of these values were used in the discrimination between the pairs and, for each pair, the classifier selected different attributes, which contributed in the best to the distinction of each case.

The SVM classifier was thus performed to evaluate the discrimination between the classes, and the confusion matrix (a specific table layout that allows visualization of the performance of algorithm, each column of the matrix represents the instances in a predicted class, while each row represents the instances in an actual class) for each pair of lesions is presented in Fig. 6.

Figure 6 shows that most of the lesions were classified correctly. SCC × AK was the pair of lesions that had the best discrimination (82.9% sensitivity and 85.7% specificity), which was already expected, since this pair of lesions was the one that showed the greatest visual difference in the thermal images.

Melanoma × PSK was the pair of lesion with less accuracy (65% sensitivity and 70% specificity), but the results were still quite satisfactory, with most lesions of both types classified correctly. This lower accuracy is due to the low incidence rate of melanoma lesions, which resulted in a low number of melanoma lesions recorded during the timespan of the study. Further, the cutaneous melanomas registered are primary and small tumors, and such melanoma lesions do not present relevant temperature increase due to its low angiogenesis stimulation.[25]

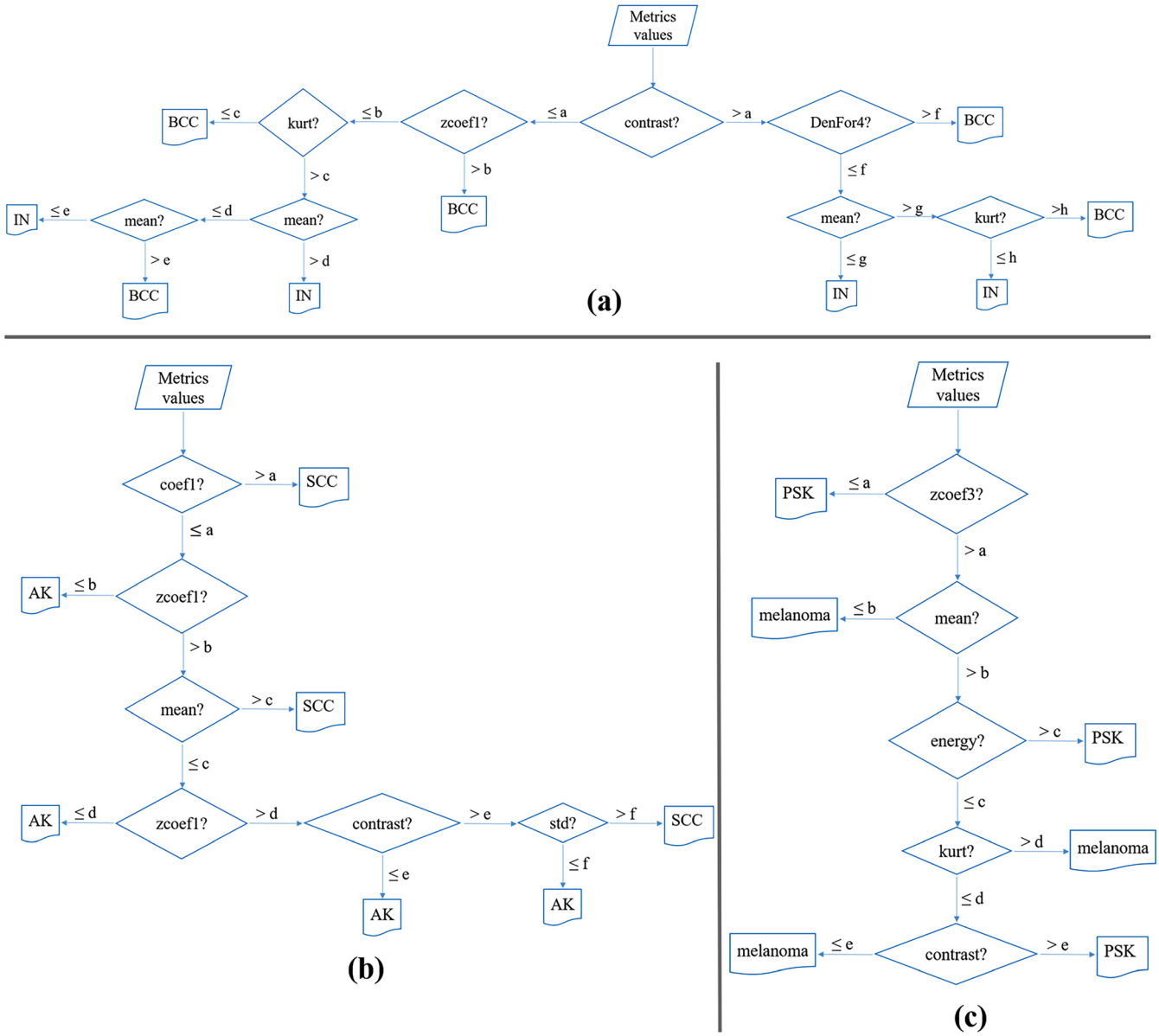

FIG. 5. The flowcharts obtained to lesions discrimination using the attributes values to (a) BCC *versus* NI; (b) SCC *versus* AK, and melanoma *versus* PSK.

Figure 7 shows the Receiver Operating Characteristic (ROC) curves of lesion pairs, which show the plotting of the true positive rate against the false positive rate.

Again, SCC × AK showed greater discrimination, since its true positive rate grows faster than in other curves. BCC × IN and melanoma × PSK have been shown to have similar true positive rate growth, showing that the method has similar discrimination abilities for both lesions. The melanoma curve × PSK presents a less homogeneous curve, with a more prominent stepwise increase in the true positive rate, as a result of having fewer lesions analyzed in each type.

The results show satisfactory discrimination capacity of clinically similar lesions, suggesting that the thermography

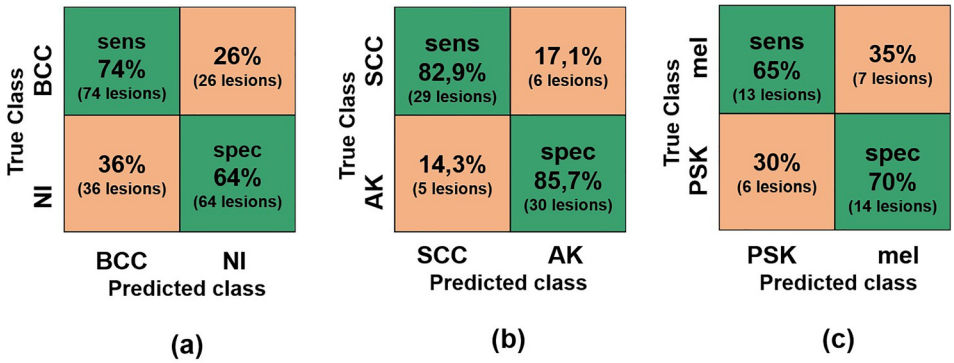

FIG. 6. Confusion matrix obtained by SVM classifier using the Weka software for the pairs (a) BCC × IN; (b) SCC × AK, and (c) melanoma × PSK. The rows show the type that the lesion is and the columns show the type that the lesion was classified. The sensitivity and specificity are indicated.

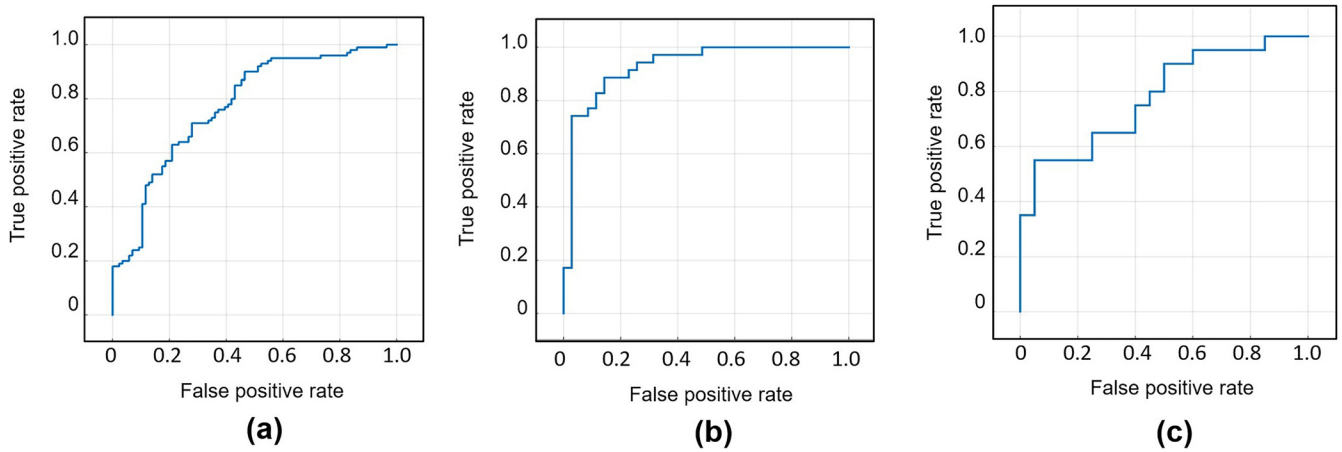

FIG. 7. ROC curves obtained by SVM classifier using the Weka software for the pairs (a) BCC × IN; (b) SCC × AK, and (c) PSK × melanoma. Greater discrimination is presented by a faster increase in the true positive rates.

can be used as a tool to help non-specialist physicians in accurately diagnosing skin lesions. Used together with dermoscopy, this method can improve the evaluation result of each technique alone.

IV. CONCLUSIONS

Thermography is a noninvasive technique completely safe to humans. Thermal images of clinically similar lesions showed significant differences between AK and SCC lesions. The SCC thermal image presented, in general, higher temperature within the lesion site and the immediately surrounding region. On the other side, thermal images of AK showed almost no temperature difference when compared to its surroundings. The pairs of clinically similar lesions, BCC *versus* nevus and melanoma *versus* PSK, presented lower temperature by the lesion site but, in general, benign lesions presented a higher definition of borders than malignant lesions, which means that the delimitation of those lesions is more clearly distinguishable by the thermal images. This observation can be justified by the fact that malignant cells usually stimulate local angiogenesis to provide tumor blood supply, and as that may provide increased metabolism for specific tumor cells, it also makes thermal diffusion more gradual as blood dissipates heat within the surrounding tissue, thus decreasing contrast between lesion and normal tissue in thermal imaging. A MATLAB® routine was used to evaluate image metrics, and SVM was used as a classifier for discrimination of lesions based on metrics values and correlation. The results showed satisfactory discrimination of clinically similar lesions, suggesting that thermography can become a diagnostic tool to auxiliary a faster screening of suspicious lesions.

ACKNOWLEDGMENTS

The authors thank the Brazilian agencies which funded this study (scholarships and facility infrastructure) via the grants Center for Research in Optics and Photonics - CePOF (Sao Paulo Research Foundation - FAPESP Grant No. 2013/07276–1), National Institute of Optics and Photonics - INCT (National Council for Research and Development - CNPq Grant No. 465360/2014–9 and Sao Paulo Research Foundation - FAPESP Grant No. 2014/50857–8), and Coordination for Improvement of Higher Education - CAPES (institutional scholarship).

The authors declare that they have no competing interests.

[1]A. Lomas, J. Leonardi-Bee, and F. Bath-Hextall, "A systematic review of worldwide incidence of nonmelanoma skin cancer," Br. J. Dermatol. **166**(5), 1069–1080 (2012).
[2]See http://www1.inca.gov.br/english for incidence of melanoma and deaths due to the disease in Brazil.
[3]R. Marks, "Squamous cell carcinoma," Lancet **347**, 735–738 (1996).
[4]R. L. Moy, "Clinical presentation of actinic keratoses and squamous cell carcinoma," J. Am. Acad. Dermatol. **42**(1), S8–S10 (2000).
[5]M. T. Fernández-Figueras, C. Carrato, X. Sáenz, L. Puig, E. Mausulen, C. Ferrándiz, and A. Ariza, "Actinic keratosis with atypical basal cells (AK I) is the most common lesion associated with invasive squamous cell carcinoma of the skin," J. European Acad. Dermatol. Venereol. **29**, 991–997 (2015).
[6]Z. Jiyad, P. O. Rourke, H. P. Soyer, and A. C. Green, "Actinic keratosis-related signs predictive of squamous cell carcinoma in renal transplant recipients: A nested case-control study," Br. J. Dermatol. **176**, 965–970 (2017).
[7]S. L. Winsey, N. A. Haldar, H. P. Marsh, M. Bunce, S. E. Marshall, A. L. Harris, F. Wojnarowska, and K. I. Welsh, "A variant within the DNA repair gene XRCC3 is associated with the development of melanoma skin cancer," Cancer Res. **60**(2), 5612–5616 (2000).
[8]V. De Giorgi, D. Massi, M. Stante, and P. Carli, "False 'melanocytic' parameters shown by pigmented seborrheic keratoses: A finding which is not uncommon in dermoscopy," Dermatol. Surg. **28**(8), 776–779 (2002).
[9]H. Kittler, H. Pehamberger, K. Wolff, and M. Binder, "Diagnostic accuracy of dermoscopy," Lancet Oncol. **3**, 159–165 (2002).
[10]A. Sorensen, S. Wolter, N. Patel, R. Hansen, and H. Price, "Dermoscopy for identification of basal cell carcinomas in basal cell nevus syndrome during carbon dioxide laser surgery," Pediatr. Dermatol. **33**(1), 109–111 (2016).
[11]G. G. Rezze, B. C. S. De Sá, and R. I. Neves, "Dermoscopy: The pattern analysis," An. Bras. Dermatol. **81**(3), 261–268 (2006).
[12]Estadão, "Mais da metade dos pacientes precisa sair de suas cidades para fazer exames no Brasil," p. 1750647, see http://brasil.estadao.com.br/noticias/geral,mais-da-metade-dos-pacientes-precisa-sair-de-suas-cidades-para-fazer-exames-no-brasil (last accessed January 13, 2017).
[13]J. R. Lacowicz, *Principles of Fluorescence Spectroscopy*, 2nd ed. (Plenum, New York, 1999).
[14]C. T. Andrade, J. D. Vollet-Filho, A. G. Salvio, V. S. Bagnato, and C. Kurachi, "Identification of skin lesions through aminolevulinic acid-mediated photodynamic detection," Photodiagn. Photodyn. Ther. **11**(3), 409–415 (2014).

[15]W. M. White, M. Rajadhyaksha, S. Gonzalez, R. L. Fabian, and R. R. Anderson, "Noninvasive imaging of human oral mucosa *in vivo* by confocal reflectance microscopy," Trans. Am. Laryngol. Rhinol. Otol. Soc. **109**(10), 1709–1717 (1999).
[16]S. González and Z. Tannous, "Real-time, *in vivo* confocal reflectance microscopy of basal cell carcinoma," J. Am. Acad. Dermatol. **47**, 869–874 (2002).
[17]R. Haddad, A. Blumenfeld, A. Siegal, O. Kaplan, M. Cohen, Y. Skornick, and H. Kashtan, "*In vitro* and *in vivo* effects of photodynamic therapy on murine malignant melanoma," Ann. Surg. Oncol. **5**(3), 241–247 (1998).
[18]N. Arora, D. Martins, D. Ruggerio, E. Tousimis, A. J. Swistel, M. P. Osborne, and R. M. Simmons, "Effectiveness of a noninvasive digital infrared thermal imaging system in the detection of breast cancer," Am. J. Surg. **196**, 523–526 (2008).
[19]T. M. Buzug, S. Schumann, L. Pfaffmann, U. Reinhold, and J. Ruhlmann, "Functional infrared imaging for skin-cancer screening," in *Proceedings of Annu. Int. Conf. on IEEE Eng. Med. Biol.* (2006), pp. 2766–2769.
[20]D. A. Kennedy, T. Lee, and D. Seely, "A comparative review of thermography as a breast cancer screening technique," Integr. Cancer Ther. **8**(1), 9–16 (2009).
[21]B. F. Jones, "A reappraisal of the use of infrared thermal image analysis in medicine," IEEE Trans. Med. Imaging **17**(6), 1019–1027 (1998).
[22]J. Kerr and N. Zealand, "Review of the effectiveness of infrared thermal imaging (thermography) for population screening and diagnostic testing of breast cancer," in *New Zealand Health Technology Assessment*, Brief Series (NZHTA, 2004), Vol. 3, Issue 3.
[23]R. Gade and T. B. Moeslund, "Thermal cameras and applications: A survey," Mach. Vision Appl. **25**, 245–262 (2014).
[24]S. E. Godoy, D. A. Ramirez, S. A. Myers, G. Von Winckel, S. Krishna, M. Berwick, R. S. Padilla, P. Sen, and S. Krishna, "Dynamic infrared imaging skin cancer screening," Infrared Phys. Technol. **70**, 147–152 (2015).
[25]A. L. Shada, L. T. Dengel, G. R. Petroni, M. E. Smolkin, S. Acton, and C. L. Slingluff, "Infrared thermography of cutaneous melanoma metastases," J. Surg. Res. **182**(1), e9–e14 (2013).
[26]I. El-naqa, S. Member, Y. Yang, M. N. Wernick, S. Member, N. P. Galatsanos, S. Member, and R. M. Nishikawa, IEEE Trans. Med. Imaging **21**(12), 1552–1563 (2002).
[27]S. Chaplot, L. M. Patnaik, and N. R. Jagannathan, "Classification of magnetic resonance brain images using wavelets as input to support vector machine and neural network," Biomed. Signal Process. Control **1**, 86–92 (2006).
[28]E. Ricci and R. Perfetti, "Retinal blood vessel segmentation using line operators and support vector classification," IEEE Trans. Med. Imaging **26**(10), 1357–1365 (2007).
[29]Fluke®, "Fluke Ti400 infrared camera," see http://en-us.fluke.com/products/infrared-cameras/fluke-ti400-infrared-camera.html. (last accessed September 29, 2016).
[30]R. C. Gonzales and R. E. Woods, *Digital Image Processing* (Addison-Wesley Publishing Company, 1993).
[31]T. Acharya and A. K. Ray, *Image Processing Principle and Applications* (John Wiley & Sons, 2005).
[32]L. da, F. da Costa, and R. M. Cesar, Jr., *Shape Analysis and Classification: Theory and Practice* (CRC Press, Inc., 2000).
[33]R. M. Haralick, K. Shanmugam, and I. Dinstein, "Textural features for image classification," IEEE Trans. Syst., Man, Cybern. **3**(6), 610–621 (1973).
[34]MathWorks®, "Graycoprops," see http://www.mathworks.com/help/images/ref/graycoprops.html (last accessed September 29, 2016).
[35]C. Cortes and V. Vapnik, "Support-vector networks," Mach. Learn. **20**(3), 273–297 (1995).
[36]D. G. Altman and J. M. Bland, "Diagnostic tests 1: Sensitivity and specificity," Br. Med. J. **308**, 1552 (1994).
[37]D. M. W. Powers, "Evaluation: From precision, recall and F-factor To ROC, informedness, markedness & correlation," J. Mach. Learn. Technol. **2**(1), 37–63 (2011).
[38]T. Fawcett, "An introduction to ROC analysis," Pattern Recognit. Lett. **27**, 861–874 (2006).
[39]A. Lallas, J. Pyne, A. Kyrgidis, S. Andreani, G. Argenziano, A. Cavaller, J. Giacomel, C. Longo, A. Malvestiti, E. Moscarella, S. Piana, F. Specchio, R. Hofmann-Wellenhof, and I. Zalaudek, "The clinical and dermoscopic features of invasive cutaneous squamous cell carcinoma depend on the histopathological grade of differentiation," Br. J. Dermatol. **172**(5), 1308–1315 (2015).
[40]M. T. Dornelas, M. F. Rodrigues, D. C. Machado, Â. M. Gollner, and A. P. Ferreira, "Expressão de marcadores de proliferação celular e apoptose no carcinoma espinocelular de pele e ceratose actínica," An. Bras. Dermatol. **84**(5), 469–475 (2009).